Article

Not peer-reviewed version

Optimizing Solar Potential Analysis in Cuba: A Methodology for High-Resolution Regional Mapping

Javier Domínguez *, Carlo Bellini, Ana María Martín, Luis F. Zarzalejo *

Posted Date: 22 August 2024

doi: 10.20944/preprints202408.1615.v1

Keywords: solar mapping; GIS; solar resources; solar radiation; renewable energies; rural electrification; sustainable development; High-Resolution Models

 doi:10.20944/preprints202408.1615.v1

Article

Optimizing Solar Potential Analysis in Cuba: A Methodology for High-Resolution Regional Mapping

Javier Domínguez [1,*], Carlo Bellini [2], Ana M. Martín [1] and Luis F. Zarzalejo [1,*]

[1] Renewable Energies Division, CIEMAT, 28040 Madrid, Spain; J.D.; javier.dominguez@ciemat.es A.M.M.; anamaria.martin@ciemat.es L.F.Z.; lf.zarzalejo@ciemat.es
[2] Department of Industrial Engineering, University of Padova, 35131 Padova, Italy; C.B.; carlo.bellini94@gmail.com
* Correspondence: javier.dominguez@ciemat.es (J.D.); lf.zarzalejo@ciemat.es (L.F.Z.)

Abstract: The development of solar energy on a regional scale necessitates a thorough understanding of available resources. Cuba, facing prolonged economic, environmental, and energy crises, urgently needs to enhance its sustainability through solar energy. While solar resource mapping is widespread, Cuba lacks extensive field measurements, often relying on models that may not be ideally suited for large regions like Matanzas province. Spanning over 12,000 km² with nearly 150 km between its northern and southern extremes, Matanzas presents challenges for high-resolution solar mapping. This study introduces a methodology that integrates various methods and databases to achieve maximum resolution in the resulting solar map. The approach is designed for large areas where conventional high-resolution models fall short. By optimizing calculation times and parameterizing the entire surface latitudinally, a high-resolution solar resource map for Matanzas has been developed. This map significantly enhances the understanding of solar resources in Cuba and proposes new methodologies for analyzing solar potential in similarly large regions.

Keywords: solar mapping; GIS; solar resources; solar radiation; renewable energies; rural electrification; sustainable development; High-Resolution Models

1. Introduction

Access to electricity is an essential requirement for human development. It is recognized as a basic need to ensure the respect of human rights and the improvement of life quality. Despite this, there are still more than 700 million people in the world without access to electricity. Unfortunately, the COVID19 pandemic has contributed to worsening these conditions. The International Energy Agency (IEA) estimates that in 2030, under the so-called STEPS scenario, some 670 million people worldwide will still be without access to electricity [1].

This highlights the pressing need to advance energy access strategies, with decentralized solutions emerging as one of the most effective and economical options. Renewable energies are crucial in addressing this challenge while ensuring sustainability. In many regions, they are also the most cost-effective choice. A key advantage of renewable energy is its global availability, even in areas where conventional energy distribution is challenging. However, its inherent variability—both temporal and spatial—can pose challenges to maintaining a reliable power supply. Therefore, a thorough assessment of the available energy mix is essential in the early stages of any electrification project. This process involves several factors, many of which are often identifiable at the local level.

Dealing with Renewable Energy Sources (RES), an adequate assessment is fundamental when working with coupling the energy demand with the power supply. Spatial and temporal variability play a crucial role in this process. In addition, the integration of a technology has always an important territorial impact, which is not easily detected by a merely technical approach. Geographic Information Systems (GIS) represents an instrument capable of integrating non-spatial features (technological, economical, etc.) in a local reality, not only intended from a geographical point of view, but also from the perspective of a network of mutually related activities [2]. In short, the wide

 doi:10.20944/preprints202408.1615.v1

geographical dispersion that characterizes RES and the importance of evaluating their integration at a local level fit perfectly with the potential of GIS analysis.

This study focuses on the development of solar maps aimed at enhancing rural electrification, providing decision-making tools based on GIS. These tools are designed to facilitate the integration of solar energy as a viable strategy to address energy access challenges while enhancing the sustainable use of local resources and supporting rural populations. The primary objective of this research is to improve the resolution of solar maps using standard methodologies. To achieve this, a case study was conducted in the Matanzas province of Cuba as part of the HIBRI2 project (Integrated Control System for Energy Supply through Hybrid Systems in Isolated Communities in Cuba, Phase II) [3,4]. This research aims to contribute to the promotion of efficient renewable energy use and development in Cuba by designing and implementing innovative systems that hybridize various technologies.

There is a wide variety of studies that highlight the value of different geographic information tools in the development of solar maps. For example, a recent work of Benalcazar [5] propose a GIS approach that combines land eligibility and techno-economic assessments for utility-scale photovoltaic systems. On another scale, with a focus on islands, Gacu [6] develops a solar power suitability map for establishing solar PV systems maximizing the full potential of their land. Other authors as Ibraheem [7], focused his research on tools and remote sensing data, provided by governmental agencies as National Aeronautics and Space Administration (NASA), that include information about direct normal irradiance (DNI) and global horizontal irradiance (GHI) data. Over these data, a GIS program was used to analyse solar irradiation, Digital Elevation Model (DEM) and land use information. This helped identify areas suitable for solar power by considering land use and topography.

In this regard, a key work is that of Kanters [8], which raises the importance of solar maps with a focus on an urban environment. In the case of Kanters and Loquias [8,9], implementation takes place in the Philippines, using GHI data in raster format with a 250 m of spatial resolution and a DEM 30 m, far from the resolution required by our research. Other authors, such as Szabó [10], use existing solar maps in raster format as a basis for a feasibility analysis on a national scale. Obviously, this requires the prior existence of such a source of information at a scale suitable for the purpose of the analysis, which is not the case here.

Authors such as Alrawashdeh emphasize the importance of solar radiation data in the design and development of solar energy projects [11]. Alrawashdeh's study, conducted on a national scale, provides valuable insights for policymakers; however, the resolution of the data may not be suitable for local-scale applications. In a similar geographic context, Settou [12] and Hasan [13] research focuses on the site selection for a specific solar PV power plant, utilizing high-resolution spatial data to optimize the process. Also in Algeria, Yaiche [14] underscores the critical role of sunshine duration in solar energy assessments. In contrast, the work of Enjavi-Arsanjani [15] shifts the focus to electricity generation through concentrated solar power (CSP) in environments similar to those in previous studies, such as Iran.

Jung [16], on the other hand, highlights the benefits of using publicly available data sources and prioritizing land with minimal competition for use in solar energy projects. The accessibility of such data is crucial for its effective application. Lastly, in the context of urban solar mapping, authors like Kanters [17] and Wegertseder [18] stress the importance of developing solar cadasters to promote solar self-consumption and optimize urban solar potential.

While Geographic Information Systems, such as ArcGIS [19], are commonly used for creating solar radiation maps, they encounter difficulties when applied to large regional maps with high metric resolution. To address this issue, a new methodology is proposed that integrates Meteonorm [20] data with ArcGIS. This approach involves tessellating the territory into smaller units and applying Meteonorm parameters to each unit. The province of Matanzas in Cuba is selected as a case study to test this methodology, given its large size and significance for solar energy development, and it has not been previously studied at this resolution.

 doi:10.20944/preprints202408.1615.v1

Dealing with solar systems modeling, an input layer was required representing the available resource. A high spatial resolution is needed, since the present work is primarily designed for small scale realities. Hence, the high-quality assessment of solar resource represents an objective of the work. The proposed approach is not limited in providing useful information for the model. A method is defined for the creation of solar radiation maps, with the purpose of being replicable for any location of interest.

2. Materials and Methods

For this study, the entire province of Matanzas (Cuba) is considered as reference area. In order to check the results, a small area in Guasasa, at the south of the province, is used as testing. The Matanzas province is located in the western region of Cuba (latitude 23° 03' 4" N and longitude 81° 34' 31" W). With an area of 11,798 km², it is the second largest province, representing 10.7% of the total area of the country. It limits with the provinces of Villa Clara, Cienfuegos and Mayabeque. The territory is characterized by the predominance of plains that occupy three quarters of the province, with the highest altitudes to the northwest and center west. The southern coast is for the most part a swampy plain. The Guasasa community (332 inhabitants) belongs to the municipality of Ciénaga de Zapata on the southeast coast of the Matanzas province. It is by the Caribbean Sea and surrounded by forests and swamps [21]. Respect to the solar potential, in the case of Cuba, the study of Prăvălie [22] highlights how most of the values are above 1,800 kWh/m² of annual global horizontal irradiation.

Several resources allow us to know the spatial distribution of solar radiation over the study area. Generally, the available maps are created through the interpolation and extrapolation of data series form measurement stations networks, combined with satellites estimations. Some of the most reliable and used [7,23–25] web map sources are the following:

- *Global Solar Atlas* is provided by World Bank and the Energy Sector Management Assistance Program (ESMAP) and was developed by Solargis [26]. This web offers information on global irradiation (horizontal, direct normal and tilted optimum angle). The raster data of average of daily totals and yearly/monthly totals are available in GeoTIFF and AAIGRID formats with a spatial resolution (pixel size) of 9 arcsec (nominally 250 m).
- *NASA Power | Prediction of Worldwide Energy Resources* supplies data of monthly and annual averages radiation (horizontal and direct normal) under real and clear sky conditions [27]. The raster data are in ASCII, csv, GeoJSON, GeoTIFF and NetCDF formats with a spatial resolution of 0.5 degrees. It also offers the option of data series for a single or a regional selected location.
- *Photovoltaic Geographical Information System (PVGIS)* [28] by the European Commission provides a free and open access database of solar radiation values for Europe, Africa and most of Asia and America. The maps available for download correspond to the monthly and annual global irradiance (horizontal, tilted to the optimum and on a two-axis sun-tracking surface). The raster data are ESRI ascii grid format with various spatial resolutions depending on the geographical coverage of the required database (CMSAF - 0.025°, SARAH - 0.05° and NSRDB - 0.04°). It also has different series of daily, monthly and annual data for a single location.

In order to determine the radiation, also data from measurement stations may be used to generate maps trough interpolating the values. Although this information may be available in yearly, monthly and daily averages series, the distribution of stations may be uneven and not all regions are covered equally [29–31]. However, dealing with small and rural areas, a more specific approach would be recommended. Isolated zones are less likely to provide direct measurements, also topographic heterogeneity affects considerably the insolation [32]. Another option is solar radiation maps generated with GIS software that model solar radiation in an area considering the factors that influence its distribution. The set of solar radiation analysis tools from ArcGIS software by ESRI calculate global radiation for a specific area, latitude and time period, taking into account atmospheric conditions and the influence of topography [33–35]. Also, the solar module *r.sun* in GRASS GIS generates raster maps of global radiation for a given day, considering a clear or cloudy sky environment [36–38]. This module which is also integrated into the QGIS software.

 doi:10.20944/preprints202408.1615.v1

This study is based on the application of the software ArcGIS version 10.8 [19] to create a solar radiation raster map of Matanzas with a spatial resolution of 30 meters. This work firstly describes the operation of the *Area Solar Radiation* tool used to determine the distribution of insolation in the geographical area [33]. Secondly, the input parameters required by the tool are detailed, focusing on the description of the Digital Elevation Model (DEM), the latitude and the determination of the parameters related to the atmospheric conditions over the years (diffuse proportion and clarity index). These parameters are validated and proposed the necessary corrections to adjust the results of solar radiation. With the defined input data, we proceed to calculate the global solar radiation (monthly and annual) in the province of Matanzas. In this task, it has been necessary to divide the study area into smaller zones for the analysis and implement a Python script to run the entire process. In addition, the solar radiation is determined for a distribution of buildings in a smaller location, the community of Guasasa.

2.1. ArcGIS Area Solar Radiation

Solar radiation distribution at global scale is determined by latitudinal gradients due to effects of Earth's rotation on its axis and translation around the sun. However, at the local level, topography is the main factor in the insolation distribution, affected by the altitude variation, orientation and shadows [39].

Area Solar Radiation is an ArcGIS tool, included in the *Spatial Analyst* extension. It implements a solar radiation model using a DEM as input. Its core is the viewshed algorithm, which allows to create maps of global, direct and diffuse radiation for a specific period of time, accounting the site latitude and elevation, shifts in solar angle, atmospheric attenuation, surface orientation and the surrounding topography. It represents an effective tool for the analysis at a local scale that may be applied in larger geographic areas, pointing out spatial and temporal variation. For this reason, *Area Solar Radiation* was chosen to create the insolation map of Matanzas.

2.1.1. Viewshed Calculation

A viewshed is the angular distribution of sky obstruction. For every specific position, it provides a raster representation of the visible sky and the sky direction obstructed by the surrounding topography and surface features. For each cell of the input DEM, the viewshed algorithm calculates the maximum angle of sky obstruction (horizon angle) for a specific set of directions around the location of interest. For all the other directions, the horizon angles are calculated using interpolation [39].

Horizon angles are then projected into a hemispherical coordinate system. Every cell of the viewshed raster grid corresponds to both a tilt angle (β), relative to the horizontal plane, and the cell azimuth angle (Υ), relative to south direction, allowing to represent a three hemisphere of directions as a two-dimensional grid. Once calculated and converted the horizon angle along the set directions, the sky view associated to each cell of the DEM reminds an upward-looking fisheye photo. Such viewsheds are then overlaid with a direct sun map and a diffuse sky map to estimate the direct and diffuse radiation. Repeating the same operation to every raster cell and combining the results will produce an insolation map.

2.1.2. Sun map and Sky map

A sun map represents the apparent position of the sun and its variation over time. It is projected in the same hemispherical coordinates as the viewshed. The sun positions, defined by zenith (θ_z) and azimuth (Ψ), are derived through astronomical equations based on the latitude location and the specific time period [40–42]. Knowing the sun position, the direct solar radiation can therefore be calculated. A time interval has to be set to define the size of the discrete sky sector that represents the sun path. Penumbral effects are also accounted, so are the solar disc size variation due to refraction near the horizon.

 doi:10.20944/preprints202408.1615.v1

Since diffuse solar radiation is spread along any sky direction, its calculation is related to a different hemispherical raster representation. A sky map represents the entire sky divided into a series of sky sector, which size depends on the number of divisions set for the calculation. Diffuse radiation can be calculated for each sky sector, defined by the zenith and azimuth angles of their centroid and assigned to an identifier value.

Combining viewshed, sun map and sky map, the unobstructed sky area is determined. Hence, the direct and diffuse solar radiations are calculated considering such area only. In particular, the proportion of visible sky is represented by the gap fraction, calculated for each sector as the number of unobstructed cells divided by the total number of cells.

2.1.3. Solar radiation calculation

The incoming global solar radiation (G_{tot}) for a given location during a specific period is calculated as the sum of direct (B_{tot}) and diffuse (D_{tot}) radiations [41,43]; the algorithm neglects the contribution of reflected radiation since its estimation is complex and it generally constitutes a small proportion of the total:

$$G_{tot} = B_{tot} + D_{tot} \quad (1)$$

B_{tot} is the sum of the direct insolation from each sun map sector ($B_{\beta,\gamma}$):

$$B_{tot} = \Sigma B_{\beta,\gamma} \quad (2)$$

D_{tot} is the sum of the diffuse insolation from each sky map sector ($D_{\beta,\gamma}$):

$$D_{tot} = \Sigma D_{\beta,\gamma} \quad (3)$$

The direct solar radiation from the sun map sector incident on a cell defined by β and Υ angles is calculated as follows:

$$B_{\beta,\gamma} = I_{SC} \cdot \tau^{m(\theta_z)} \cdot SunDur_{\beta,\gamma} \cdot SunGap_{\beta,\gamma} \cdot cos(\theta) \quad (4)$$

where: I_{SC} is the Solar Constant, representing the solar flux outside the atmosphere. The value considered is at the mean earth-sun distance and, according to the World Radiation Center (WRC) with a value of 1367 W/m² [44]; τ is the transmittance of the atmosphere (averaged over all the wavelengths); θ_z is the zenith angle; $SunDur_{\beta,\gamma}$ is the equivalent time duration of the sky sector; $SunGap_{\beta,\gamma}$ is the gap fraction of the sun map sector; θ is the angle of incidence between a line collinear with the sun's rays and the normal to the surface calculated following [40,41,45]:

$$\theta = arcos[cos(\beta) \cdot cos(\theta_z) + sin(\beta) \cdot sin(\theta_z) \cdot cos(\psi - \gamma)] \quad (5)$$

and $m(\theta_z)$ is the relative optical air mass, the ratio between the length of the optical path described by the solar photons along the oblique trajectory and the length of the optical atmospheric path in the zenith direction. For zenith angles up to 89° it can be calculated by the following equation [43,46]:

$$m(\theta_z) = \frac{e^{-0.0001184 \cdot h}}{cos(\theta_z) + 0.50572\ (\theta_z + 6.07995)^{-1.6364}} \quad (6)$$

where h is the ground elevation above the sea level.

The diffuse solar radiation from the sky map sector incident on a cell is calculated as follows.

$$D_{\beta,\gamma} = P_{dif} \cdot G_n \cdot Dur \cdot SkyGap_{\beta,\gamma} \cdot Weight_{\beta,\gamma} \cdot cos(\theta) \quad (7)$$

where: P_{dif} is the diffuse proportion, indicating the fraction of global normal radiation which is diffuse; G_n is the global normal radiation; Dur is the time interval for analysis; $SkyGap_{\beta,\gamma}$ is the gap fraction for the sky sector; $Weight_{\beta,\gamma}$ is the proportion of diffuse radiation related to a sky sector with respect to all the sectors.

The global normal radiation calculable as the sum of the direct radiation from every sector without correction for angle of incidence and divided by the proportion of direct radiation ($1 - P_{dif}$):

$$G_n = \frac{I_{SC}\ \Sigma\left(\tau^{m(\theta_z)}\right)}{1 - P_{dif}} \quad (8)$$

 doi:10.20944/preprints202408.1615.v1

For the uniform sky diffuse model, it is calculated as:

$$Weight_{\beta,\gamma} = \frac{(cos\theta_2 - cos\theta_1)}{Div_{azi}} \quad (9)$$

For the standard overcast sky model, it is calculated as:

$$Weight_{\beta,\gamma} = \frac{(2 \cdot cos\theta_2 + cos2\theta_2 - 2 \cdot cos\theta_1 - cos2\theta_1)}{4 \cdot Div_{azi}} \quad (10)$$

where: θ_1 and θ_2 are the bounding zenith angles of the sky sector and Div_{azi} is the number of azimuthal divisions of the sky sector.

2.2. Input data settings

The *Area Solar Radiation* tool requires some user-defined input parameters [33]. For the present study, the parameters are set aiming a good trade-off between accuracy of results and a reasonable calculation time. Input raster (DEM), latitude, diffuse proportion and transmissivity will be introduced in the next sections. The rest of the input settings are introduced in Table 1, where:

- The Sky size defines the resolution of the viewshed, the sun map and the sky map rasters. Its value refers to the number of grid cells per side (rows and columns). A value of 200 is therefore chosen for the sky size, being a good compromise between time consumption and accuracy.
- The time configuration specifies the time for which insolation is to be calculated. The chosen periods are monthly intervals, selecting the number of start and end day out of 365 (366 for leap years, as in the case of 2020). Notice that the end day is exclusive in the period considered (e.g. January start-end days are: 1-32).
- The time interval is used for the calculation of sky sectors for the sun map. To ensure a high precision, a daily interval through the year and a 0.5-hour interval through the day has been chosen.
- Selecting "Flat Surface" option, the calculation will be performed considering the irradiation on a horizontal surface.
- The Z factor has the function to convert the surface z units when they differ from the ground x, y units. Converting all the data in a meters projected coordinate system, Z factor can be set with the value of 1.
- The number of directions refers to the viewshed calculation. For a natural terrain at 30-meters resolution so fewer directions are sufficient (16 or 32).
- The values of azimuth and zenith divisions, used to create sky sectors in the sky map, needs to be a multiple of 8.
- Selecting the "Standard Overcast Sky" diffuse model type, the incoming diffuse radiation flux varies with the zenith angle.

Table 1. Input settings for the solar analysis.

Input	Value
Sky size / Resolution	200 cells
Time configuration	Multiple days in a year (2020, Start day, End day)
Day interval	3 days
Hour interval	0.5 hours
Z factor	1
Slope and aspect input type	Flat Surface
Calculation directions	32 directions
Sky zenith divisions	16 divisions
Sky azimuth divisions	16 divisions
Diffuse model type	Standard Overcast Sky

 doi:10.20944/preprints202408.1615.v1

2.2.1. Digital elevation model

A DEM is a data set composed by points or grid cells associated to latitude-longitude location references and the respective value of altitude. It is possible to make a distinction between two types of models: Digital Terrain Model (DTM) and Digital Surface Model (DSM). While the first one refers exclusively to the ground surface, a DSM also includes vegetation and anthropic elements. The main index of DEM quality is its cell resolution. Of course, minimizing the topographic generalization is a key step in order to obtain a high-quality calculation [47].

The "Advance Land Observation System (ALOS) World 3D – 30 m (AW3D30) Digital Surface Model" is the input elevation surface data selected for this case study. This is a global digital surface model dataset with a horizontal resolution of approximately 30 m (1 arcsec). It was released in 2015 by the Japan Aerospace Exploration Agency (JAXA) Earth Observation Research Centre, in a free of charge version available upon registration [48]. A mosaic of the area formed by five tiles which includes the province of Matanzas (N022W081, N022W082, N022W083, N023W081 and N023W082) has been downloaded and properly cut and merged through ArcGIS tools. Since the insolation is influenced by the horizon angle, which depends on the surrounding topography, the area considered was extended beyond the borders of the province itself.

In Figure 1, the DEM used as input raster for the solar radiation calculation. Each pixel of the map represents an area of 30x30 meters approximately. To highlight the effective study area, a map of the province of Matanzas was overlaid.

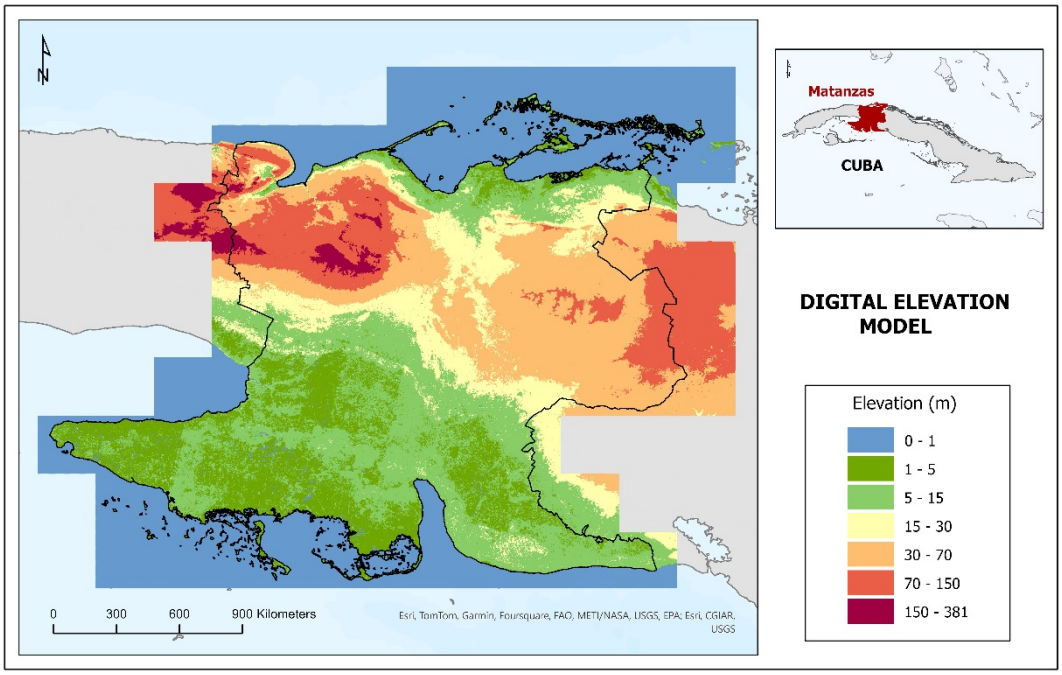

Figure 1. DEM of the province of Matanzas.

2.2.2. Latitude

The site latitude is automatically set based on the geographic coordinates of the centroid of the DEM uploaded. This solar radiation tool was mainly designed for local scales and if the study area is small, considering the same latitude for every cell is an acceptable approximation in the calculation of solar position and declination. When large areas such as regions, countries or continents are analyzed, the latitude can vary considerably between the different areas, affecting the results of solar radiation. The tool does not allow to set multiple values of latitude, therefore, the large geographical areas have to be divided into smaller study areas with different latitudes (no greater than 1 decimal degree) [33]. The same consideration is valid for the clearness index and diffuse ratio, a single value per zone, so both parameters will be determined for each of the divisions. The province of Matanzas, that is a substantially larger area, was divided into smaller subareas for this purpose. The DEM

 doi:10.20944/preprints202408.1615.v1

presented in Figure 2, has been divided into 80 squared rows with a size of 0.15x0.15 decimal degrees. Each block has been numbered proceeding from west to east and from south to north. This is one of the fundamental and most innovative aspects of the method proposed in this research.

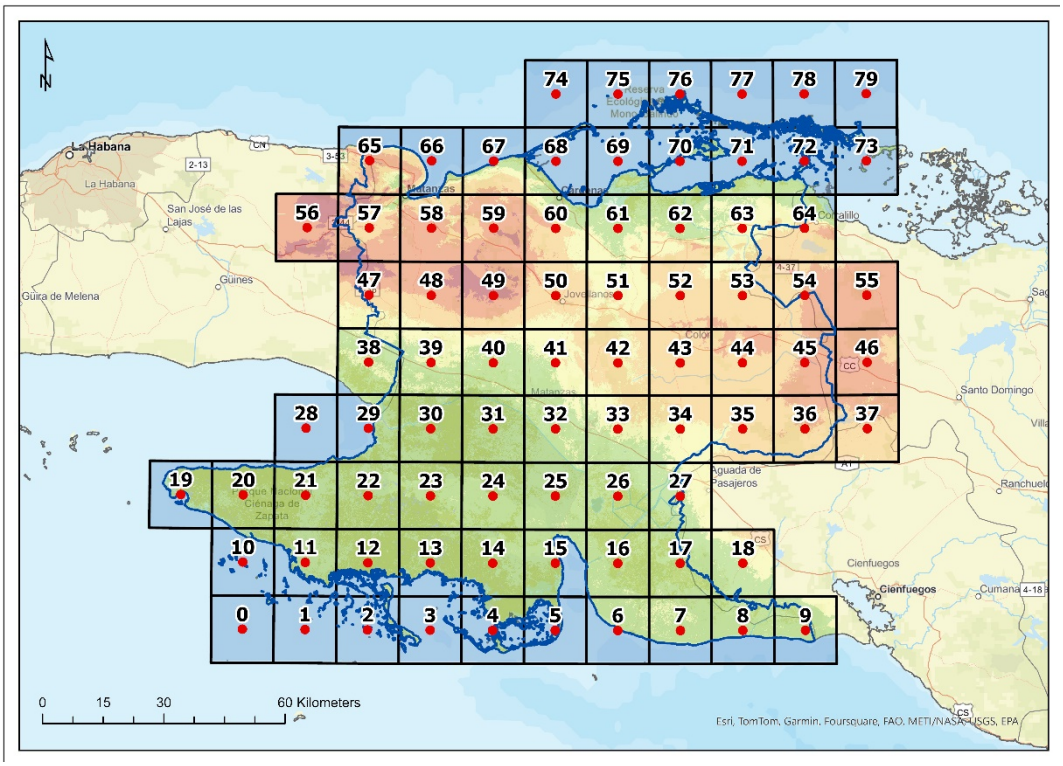

Figure 2. Matanzas province DEM including division for further analysis.

2.2.3. Diffuse proportion and clearness index

Crossing the atmosphere and colliding against its molecules and particles, a portion of the solar flux is affected by phenomena of absorption and scattering. This interaction is responsible for the attenuation of the solar radiation hitting the Earth's surface and involves gases (CO_2, O_2, O_3, other air molecules), solid particulate matter, liquid particles (aerosols, including non-condensed water) and clouds (condensed water) [49]. The influence of this factors is higher when the probability of interaction with the solar flux increases, so it depends on the distance crossed by the sunbeams, the variability in air composition (e.g. due to pollution) and weather conditions.

Area Solar Radiation tool does not consider the variability of atmospheric conditions in time and space, a limitation highlighted by the developers themselves [39]. In order to deal with this aspect, the current analysis set different values of input clearness index, diffuse proportion for each of the 80 divisions, and in relation to the period considered, thus bringing novelty to the proposed methodology.

The *diffuse proportion or cloudiness index* (K_D) is defined as the ratio of the diffuse solar radiation to the global solar radiation measured at the Earth's surface. The values range of diffuse proportion is considered in ArcGIS from 0 to 1, depending on the atmospheric conditions. Usually a value of 0.2 is considered for very clear sky conditions and 0.3 for clear sky conditions. It can be calculated [40,50] as:

$$K_D = \frac{D_{tot}}{G_{tot}} \quad (11)$$

In the case of *clearness index or atmospheric transmissivity* (K_T), it is considered as the ratio of the global solar radiation measured at the Earth's surface to the extra-terrestrial solar radiation at the top of the atmosphere. Values range from 0 (no transmission) to 1 (complete transmission). Typically observed values are 0.6 or 0.7 for very clear sky conditions and 0.5 for only a generally clear sky. The

 doi:10.20944/preprints202408.1615.v1

clearness index has an inverse relation with the diffuse proportion parameter [33] and it is calculated [40,50] as:

$$K_T = \frac{G_{tot}}{I_{SC} \cdot \varepsilon \cdot cos(\theta_z)} \quad (12)$$

where: ε represents the Earth's orbit eccentricity relative to the *n-th* day of the year, calculated as [40,45]:

$$\varepsilon = 1 + 0.0334 \cdot \cos\left(n \cdot \frac{2\pi}{365.25}\right) \quad (13)$$

The scientific literature proposes many models for the estimation of the K_T and K_D, influenced by the stochastic nature of cloud attenuation process. Statistical time series models can be reliable to forecast the clearness index in the long term, while that more recent forecasting models, based on machine learning approaches, are more effective for short term predictions [51]. The atmospheric transmissivity, according to the Lambert-Beer Law of radiation extinction, has an inverse exponential relationship with the atmospheric optical depth, which is the sum of the optical depth of each atmosphere components [52]. However, due to complexity and lack of data, which in this analysis should be spatially distributed, an empirical approach was preferred. Starting from historical data of solar radiation is possible to derive the monthly average clearness index and diffuse ratio related to each considered area.

The calculation of the monthly mean values of K_T and K_D requires monthly mean global horizontal and diffuse radiation data for the 80 selected areas represented by the centroid coordinates (Figure 2). To obtain these values, the Meteonorm software has been used [20,53]. Meteonorm is a comprehensive meteorological database containing climatological data for solar engineering applications anywhere in the world. This software combines a large data set from all over the world with numerous computational models, being able to generate statistically representative meteorological sequences for the desired location typical meteorological year (TMY).

The radiation database refers to 20 years measurements periods, while the others meteorological parameters are based on monthly averages calculated over 1961-1990 and 2000-2009 periods. Such weather stations data are adapted to every location through space dependent interpolation, considering altitude, topography, region, etc. In particular, for global radiation the interpolation procedure is a 3D inverse distance model (Shepard's gravity interpolation). Diffuse radiation is derived from global radiation through the dynamic model of Perez [54] which takes into account its anisotropic behavior concentrated in the circumsolar zone and near the horizon [40].

Once imported the list of 80 locations using the batch mode function of Meteonorm, the calculation settings have to be defined:

- The field "Future" has been selected as climatological time period, allowing to choose between three different future scenarios from the IPCC report 2007 [55]: B1 (low), A1B (mid), A2 (high). The option A1B (year 2020) has been chosen, characterized by a forecast of a more integrated world, with a balanced emphasis on all energy sources.
- The field "Interpolated" has been set for the atmospheric turbidity, basing on satellite data from the satellite experiment MISR and MODIS [53].
- A personalized output format has been selected, setting monthly global, diffuse and extraterrestrial radiation as output format of the calculation.

In the first step of the calculation, the software searches for the closest weather stations to each selected location and their long-term monthly means are interpolated. The whole set of weather station used by the current calculation are the following: La Fe, Havana/Jose Marti, Casa Blanca, Camaguey, Key West FL. In a second step, a stochastic weather generator to create a TMY of data with the selected time resolution (hourly) runs the interpolated monthly data. The results have finally been exported and used to calculate the monthly mean K_T and K_D value for each location, using (Eq.11) and (Eq.12).

 doi:10.20944/preprints202408.1615.v1

3. Results

The first key outcome of this study is the successful application of the methodology outlined in the previous section. This approach demonstrates how enhanced accuracy can be achieved through the effective combination of a tessellation procedure with a specific parameterization. This parameterization is derived from an external database, in this case, solar radiation data sourced from ArcGIS.

Secondly, we present two comparative maps illustrating the cartographic outcomes of our methodology. The first map displays solar radiation data for the entire province, showcasing a large geographical area typically not analyzed with such high resolution. This territory possesses significant potential for solar energy utilization due to its specific characteristics. The second map focuses on the detailed analysis of a smaller locality, Guasasa. This area was selected because it lies outside the established electricity grid and represents a promising candidate for autonomous electrification using renewable energy sources.

3.1. Validation and corrections of diffuse proportion and clearness index

The values of K_T and K_D need to be validated before being used as clearness index and diffuse proportion input for the execution of *Area Solar Radiation*. An effective method to validate these parameters is to run the solar radiation calculation and compare the outputs with the results provided by Meteonorm, which represents a reliable source, according to the previous section.

For this task *Point Solar Radiation* is an ArcGIS tool [56] belonging to the same *Spatial Analyst* extension as *Area Solar Radiation*. The required input parameters and the equations used are the same for both, except the location where the calculation is run: *Point Solar Radiation* derives incoming solar radiation for specific locations that can be loaded in the format of point feature class or table of point coordinates. This implies short calculation time and allows to compare directly the results with the expected values.

Like in Meteonorm calculation, the centroid coordinates of each of the 80 zones is set as input location for a *Point Solar Radiation* calculation. At this point, the main issue is the necessity of running a calculation with multiple input setting with a tool which only allows to set a unique value of clearness index and diffuse proportion.

The problem can be solved implementing a Python script that cyclically executes for the 80 grid central points, the function *Point Solar Radiation* from the "arcpy" environment. The script is run for every month of the year and sequentially load the DEM raster file of the zone in which the point is located, its latitude and the monthly K_T and K_D values. Once calculated the monthly global, direct and diffuse radiation for each of the 80 points, the outputs are merged into three single files.

The output radiation generated by the script execution differs significantly from the value estimated by Meteonorm. The monthly mean error, calculated as a percentage of the Meteonorm values and averaged for all the 80 study areas, is presented in table 2 separating global (err% glob), direct (err% dir) and diffuse (err% diff) radiation.

Table 2. Error mean percentage of the Point Solar Radiation calculation in relation to the monthly Meteonorm values.

	Jan.	**Feb.**	**Mar.**	**Apr.**	**May.**	**Jun.**	**Jul.**	**Aug.**	**Sep.**	**Oct.**	**Nov.**	**Dec.**
err% glo	-8.7	12.0	18.6	23.9	30.1	23.5	30.4	37.2	35.4	21.9	-0.4	-20.0
err% dir	-12.2	17.6	28.9	39.9	46.5	30.5	46.2	57.4	54.3	32.1	-1.4	-36.9
err% diff	-2.7	4.7	4.0	0.8	10.2	16.7	11.5	16.3	18.9	12.5	1.7	1.1

As can be noticed in Eq. 4, the calculation of direct radiation depends on a fixed solar constant, without taking into account how the Earth's orbital eccentricity influences the incoming irradiance. Considering the effect of the Sun distance variability over the year (Eq. 13) represents a first correction factor to reduce the error. Using the equations [40,45] to calculate the extraterrestrial normal radiation $I_{0,n}$:

$$I_{0,n} = I_{sc} \cdot \varepsilon \tag{14}$$

 doi:10.20944/preprints202408.1615.v1

Taking into account that for each month we must use the middle day of every month as n input value in Eq. 14. Accounting the eccentricity effect on direct radiation direct results to have an effect of mitigation of the error as can be seen in Table 3:

Table 3. Error mean percentage of the 80 Point Solar Radiation calculations, accounting the eccentricity effect, compared to the monthly Meteonorm values.

	Jan.	Feb.	Mar.	Apr.	May.	Jun.	Jul.	Aug.	Sep.	Oct.	Nov.	Dec.
err% glo	-5.8	14.5	19.7	22.9	27.2	19.6	26.3	34.0	34.3	22.9	1.9	-17.5
err% dir	-9.6	20.3	30.1	38.8	43.2	26.4	41.6	53.8	53.0	33.2	0.9	-34.9
err% diff	-0.5	7.0	5.0	0.0	7.7	13.0	7.9	13.5	17.9	13.5	4.0	4.3

A correction of the input values of clearness index and diffuse proportion is still needed to minimize the discrepancy and achieve a better accuracy. The clearness index input required by the ArcGIS tool refers to a condition of zero altitude, while the calculated K_T refers to the actual conditions of the respective sites. An average error was therefore predictable. However, the existing heterogeneity across the different areas reflects a good approximation of the variability due to weather conditions forecast. Applying the same correction factor to every area, such variability accuracy is preserved.

A first step is focused on minimizing the percentage error of direct radiation. The K_T values have been modified with a per cent variation of ±5% and different execution of the script have been done, investigating the modified K_T which produces the most accurate direct radiation output (in comparison to Meteonorm values) for each month. In Table 4, the errors of the outputs produced by using $K_{T,mod}$ and K_D as input of the calculation, where $K_{T,mod}$ is the clearness index value, which minimizes the direct radiation error. The second row shows the applied variation from the original K_T values.

Table 4. Error mean percentage of the 80 Point Solar Radiation calculations compared to the monthly Meteonorm values, using the modified clearness index ($K_{T,mod}$) as input transmissivity.

	Jan.	Feb.	Mar.	Apr.	May.	Jun.	Jul.	Aug.	Sep.	Oct.	Nov.	Dec.
K_T mod	+5%	-10%	-20%	-20%	-25%	-15%	-25%	-30%	-25%	-15%	-	+25%
err% glo	2.6	-2.7	-9.5	-8.1	-12.0	-3.0	-7.8	-15.4	-9.2	-4.2	1.9	25.6
err% dir	-1.7	2.8	-0.5	3.0	0.1	3.2	-1.2	-1.6	4.3	4.4	0.9	-1.4
err% diff	9.5	-9.8	-22.3	-27.0	-27.2	-9.5	-27.0	-30.0	-21.9	-12.6	4.0	58.4

Diffuse radiation is calculated depending on global normal radiation G_n (Eq. 8) which also depends on direct radiation, as can be seen in Eq. 8. For this reason, direct radiation needs to be corrected first. A second step is to minimize the gap of diffuse radiation. Following the same procedure, modified values of K_D with per cent variation of ±5% have been tested, coupled with $K_{T,mod}$ as input of the point solar radiation script. The chosen couples of $K_{T,mod}$ and $K_{D,mod}$ are the ones that produced the minimum error, as reported in the Table 5.

The second row shows the applied variation respect the original K_T and K_D values, respectively.

A comparison is useful to visualize the trend and the correction. The monthly global, direct and diffuse horizontal irradiation has been calculated for the 80 point-locations identified along the province of Matanzas. The average values between the 80 locations have been used to compare the output calculated by Point Solar Radiation with the reference values calculated by Meteonorm. Properly adjusting the input values of K_T and K_D, the error between the two calculations has been minimized.

Table 5. Error mean percentage of the 80 Point Solar Radiations calculation compared to the monthly Meteonorm values, using the modified clearness index ($K_{T,mod}$) as input transmissivity and the modified diffuse ratio ($K_{D,mod}$) as input diffuse proportion.

	Jan.	Feb.	Mar.	Apr.	May.	Jun.	Jul.	Aug.	Sep.	Oct.	Nov.	Dec.
K_T mod	+5%	-10%	-20%	-20%	-25%	-15%	-25%	-30%	-25%	-15%	-	+25%

 doi:10.20944/preprints202408.1615.v1

K_D mod	-5%	+5%	+15%	+15%	+20%	+5%	+20%	+20%	+10%	+5%	-	-25%
err% glo	-0.8	1.0	-0.2	0.7	2.0	1.5	1.6	0.9	0.3	0.6	1.9	-1.4
err% dir	-1.7	2.8	-0.5	3.0	0.1	3.2	-1.2	-1.6	4.3	4.4	0.9	-1.4
err% diff	0.8	-1.4	0.0	-6.4	4.2	-0.3	4.8	3.6	-3.6	-3.2	4.0	-1.5

In the following tables and graphs, "Point solar" refers to the outputs calculated before the correction, while "Corrected" refers to the outputs calculated using the modified $K_{T,mod}$ and $K_{D,mod}$.

Table 6. Monthly global horizontal irradiation calculated through: Meteonorm (first row), Point Solar with original values of K_T and K_D (second row), Point Solar with corrected values $K_{T,mod}$ and $K_{D,mod}$ (third row).

Global Horizontal Irradiation (kWh/m²)												
	Jan.	**Feb.**	**Mar.**	**Apr.**	**May.**	**Jun.**	**Jul.**	**Aug.**	**Sep.**	**Oct.**	**Nov.**	**Dec.**
Meoteonorm	121.6	129.3	167.8	182.7	187.4	170.6	186.1	172.7	145.0	130.8	118.9	107.7
Point Solar	111.0	144.8	199.0	226.4	243.9	210.7	242.7	237.0	196.4	159.4	118.4	86.1
Corrected	120.6	130.5	167.4	184.0	191.3	173.1	189.1	174.4	145.5	131.6	121.2	106.1

Table 7. Monthly direct horizontal irradiation calculated through: Meteonorm (first row), Point Solar with original values of K_T and K_D (second row), Point Solar with corrected $K_{T,mod}$ and $K_{D,mod}$ (third row).

Direct Horizontal Irradiation (kWh/m²)												
	Jan.	**Feb.**	**Mar.**	**Apr.**	**May.**	**Jun.**	**Jul.**	**Aug.**	**Sep.**	**Oct.**	**Nov.**	**Dec.**
Meoteonorm	74.6	73.1	98.5	108.8	104.6	88.0	103.1	89.6	71.0	64.7	57.5	59.5
Point Solar	65.5	86.0	127.0	152.2	153.2	114.9	150.7	141.0	109.5	85.5	66.6	37.5
Corrected	73.4	75.2	98.1	112.1	104.7	90.8	101.9	88.2	74.0	67.6	68.1	58.6

Table 8. Monthly diffuse irradiation calculated through: Meteonorm (first row), Point Solar with original values of K_T and K_D (second row), Point Solar with corrected values $K_{T,mod}$ and $K_{D,mod}$ (third row).

Diffuse Irradiation (kWh/m²)												
	Jan.	**Feb.**	**Mar.**	**Apr.**	**May.**	**Jun.**	**Jul.**	**Aug.**	**Sep.**	**Oct.**	**Nov.**	**Dec.**
Meoteonorm	47.0	56.2	69.4	74.1	83.0	82.5	83.2	83.1	74.1	66.2	51.3	48.3
Point Solar	45.7	58.8	72.2	74.7	91.4	96.3	92.7	96.7	88.0	74.4	52.1	48.8
Corrected	47.4	55.4	69.3	69.4	86.5	82.3	87.1	86.1	71.4	54.0	53.3	47.5

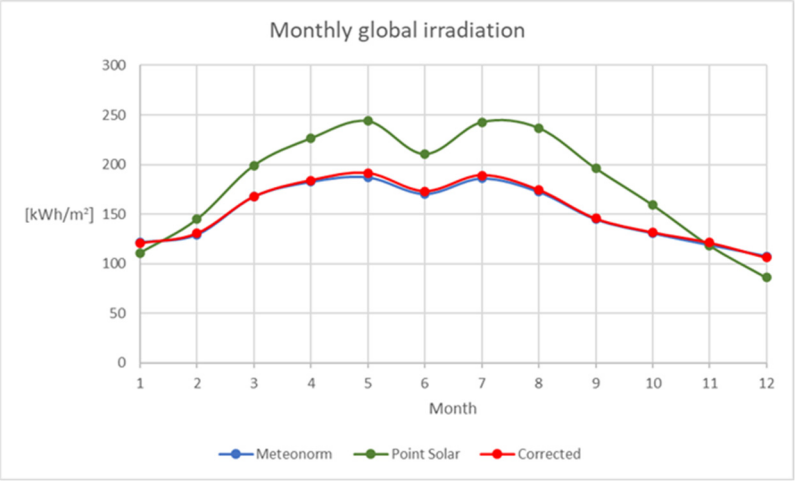

Figure 3. Trend of the monthly global horizontal irradiation calculated through: Meteonorm (blue), Point Solar with original values of K_T and K_D (green), Point Solar with corrected values K_T and K_D (red).

Preprints.org (www.preprints.org) | NOT PEER-REVIEWED | Posted: 22 August 2024 doi:10.20944/preprints202408.1615.v1

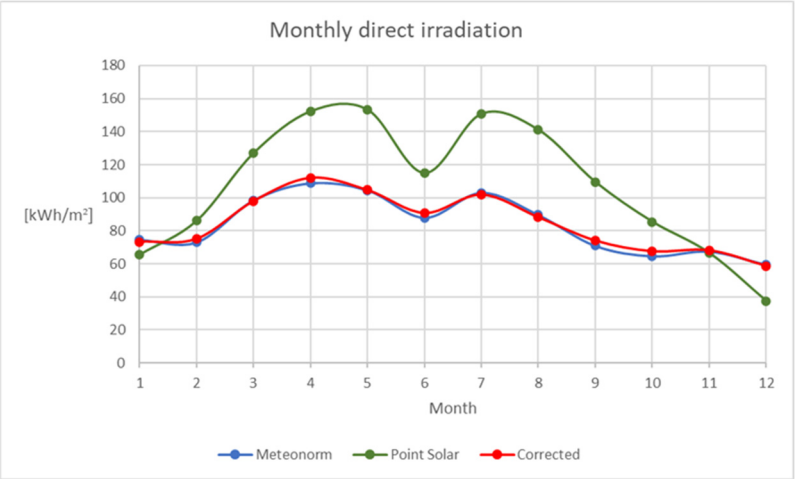

Figure 4. Trend of the monthly direct horizontal irradiation calculated through: Meteonorm (blue), Point Solar with original values of K_T and K_D (green), Point Solar with corrected values K_T and K_D (red).

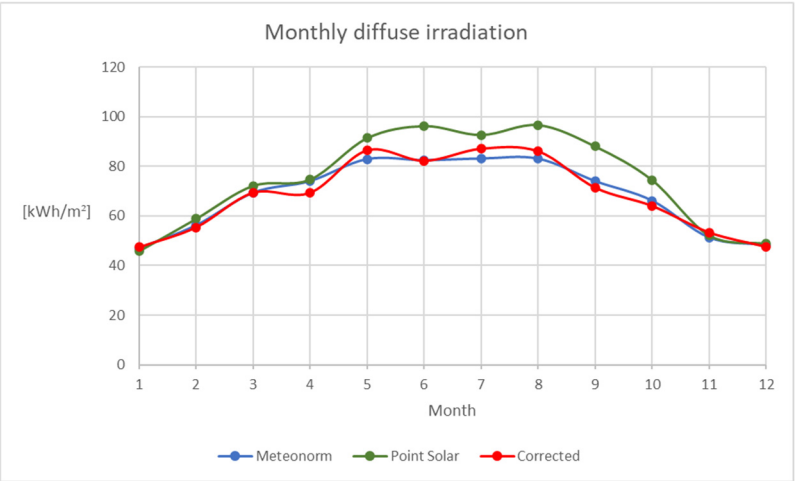

Figure 5. Trend of the monthly diffuse irradiation calculated through: Meteonorm (blue), Point Solar with original values of K_T and K_D (green), Point Solar with corrected values K_T and K_D (red).

3.2. Matanzas province solar radiation map

Once the input parameters required by *Area Solar Radiation* tool are provided, it is possible to proceed to the creation of the solar maps. In the same way as *Point Solar Radiation* tool, a script is required to run the calculation with different inputs for each zone. The two scripts have a similar structure: a number of fixed input settings are combined to variable input settings which are iteratively taken from the parameters of a single zone: latitude, clearness index and diffuse proportion. In addition to them, the script set the extent of the portion of total raster DEM that will be processed by the tool. For each loop generated by the script, the extent area needs to be defined by setting the coordinates of their opposite corners. Every time the command is executed, it generates a portion of global solar map. When the loop comes to the last iteration all the portions are merged in a single raster by the tool *Mosaic to new raster*. The setting chosen for the mosaic are: pixel type 32_BIT_FLOATING; number of bands 1; mosaic method MEAN; mosaic color map mode FIRST. This means that the output cell values of the overlapping areas are the average value of the overlapping cell and the color map of the first raster dataset will be applied to all the raster mosaic. The extent environment borders exceeds the size area of each zone, in order to flatten the gap between

 doi:10.20944/preprints202408.1615.v1

contiguous areas. The 80 zones identified have a size of 0.15x0.15 decimal degrees, while the chosen size of the extent area is 0.225x0.225 decimal degrees.

Finally, the resulting monthly solar maps of Matanzas are summed and merged. The map obtained (Figure 6) represents the Annual Global Horizontal Irradiation in Matanzas. The high-resolution is hidden by the large scale of the area considered. A closer view would highlight the variation of the solar radiation pixel by pixel. In the northern part of the province, characterized by a mountain landscape, a higher level of radiation is visible along the slopes. The relevance of this result is that any portion of this wide area can be extracted and used for eventual future studies.

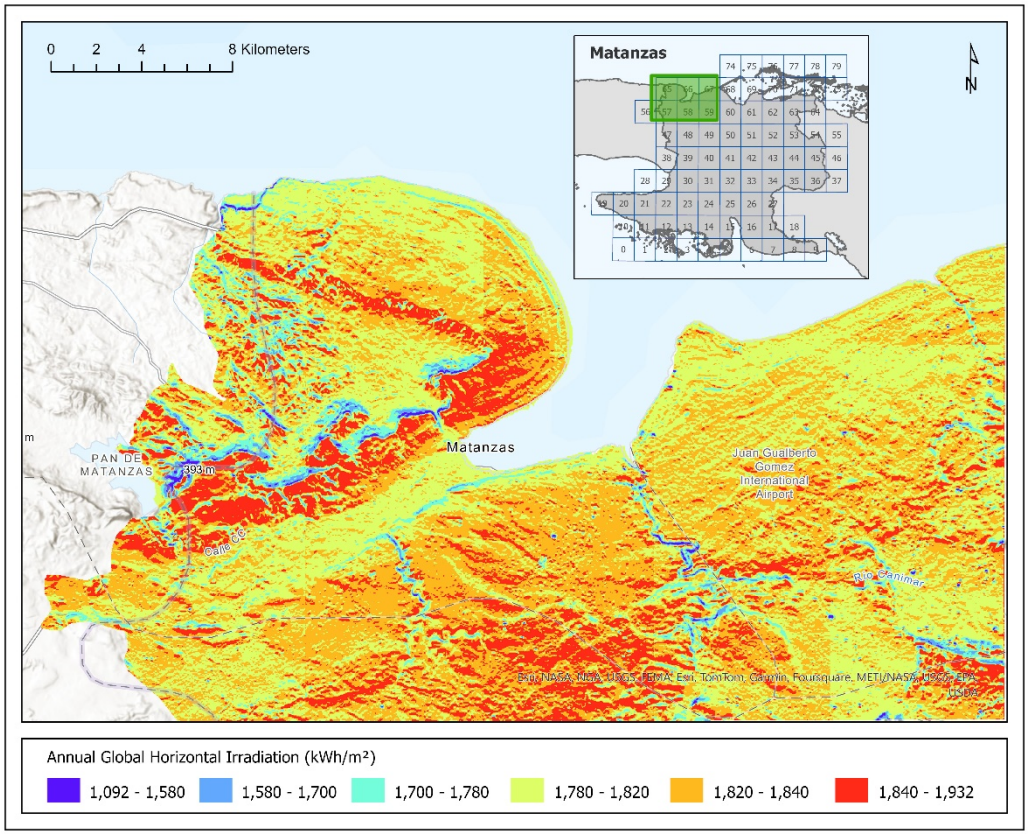

Figure 6. Annual Global Horizontal Irradiation in Matanzas.

3.3. Guasasa solar radiation map

To conclude, from the solar radiation map of the province of Matanzas we have to obtain the radiation values on the study area over the community of Guasasa. The calculated map of Matanzas is referred to the global horizontal irradiation (G_H) and it is necessary to determine the radiation available for a PV installation in the buildings distribution of the community. The assessment of the PV potential requires as input the solar radiation received by the solar panel surface, so on a tilted surface. The surface angle considered is the optimal tilt angle (β_{opt}). In order to calculate the global irradiation on optimal tilted surface a correction factor is needed.

Setting the coordinates of Guasasa in the PVGIS web [28], the monthly average values of average values of G_H and $G_{\beta opt}$ are downloaded. The period considered for the data collection is from 2001 to 2020. The ratio of each couple of values is calculated and the average value of each ratio is considered as correction factor K_β:

$$K_\beta = \frac{G_{\beta_{opt}}}{G_H} = 1.088 \quad (15)$$

As shown in figure 7, by multiplying the factor K_β for each pixel of the annual G_H raster, a new raster representing the $G_{\beta opt}$ is obtained.

Preprints.org (www.preprints.org) | NOT PEER-REVIEWED | Posted: 22 August 2024 doi:10.20944/preprints202408.1615.v1

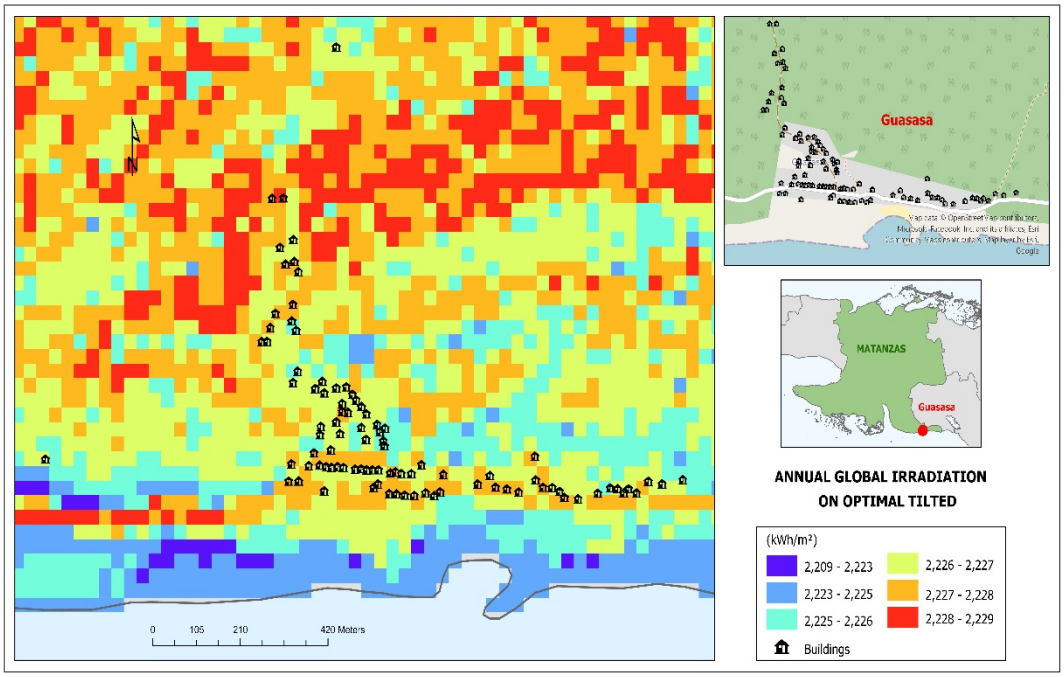

Figure 7. Annual Global Irradiation on optimal Tilted Surface in Guasasa (Matanzas).

4. Discussion and Conclusions

A series of twelve maps, one for each month of the year, are created and merged in order to provide a value for each pixel of the average annual radiation received. The shadows originated by both the morphology and the horizon characteristics are considered in the calculation. The study includes the implementation of a python script for the cyclic execution of *Area Solar Radiation*, with the aim of bypassing the limitation of the tool in performing the calculation for large areas. Indeed, the input settings only allows the insertion of single values for the definition of the atmospheric influence on solar radiation, a condition which may vary considerably over time and space. The validation is conducted through the software Meteonorm, version 7.

Meteonorm is a widely used solar radiation data source in the solar energy industry. Its reliable database provides punctual values of solar radiation for any desired site. Selecting an adequate number of locations, it is possible to compare the results with the output derived from the ArcGIS calculation. In order to facilitate the comparison, a second python script is implemented for the cyclical execution of *Point Solar Radiation*, another ArcGIS tool. It has the same architecture of *Area Solar Radiation* but designed for the calculation on specific point locations. The comparison allows to investigate and perform the necessary corrections on the input tool settings, so that the output of *Area Solar Radiation* have a minimal error respect to the experimental measurements.

This development presents a high-resolution solar radiation map for Matanzas, Cuba, utilizing a novel methodology to enhance accuracy in solar radiation calculations over extensive areas. The study highlights the potential of commercial software for solar radiation analysis across various scales, demonstrating how precise application requires adapting parameters to the specific conditions of the study area and validating results against other available databases or programs. The development and implementation of customized scripts, as illustrated by our methodology, can significantly improve accuracy and relevance. Thus, the approach presented here not only advances solar radiation mapping for Matanzas but also serves as a valuable reference for similar studies aiming to refine solar energy assessments in diverse contexts.

Author Contributions: Direction of the research, J.D. and L.F.Z.; Conceptualization, J.D. and L.F.Z.; methodology, J.D., C.B., A.M.M. and L.F.Z.; software and validation, C.B. and A.M.M.; writing—original draft preparation, C.B. and J.D.; writing—review and editing, all authors; scientific supervision, J.D. and L.F.Z.; project

administration, J.D.; funding acquisition, J.D. All authors have read and agreed to the published version of the manuscript.

Funding: This research was funded by the Spanish Agency for International Development Cooperation (AECID), grant number 2018/ACDE/000600, under the innovation action HIBRI2, and by the ERASMUS + program of the European Union (I-PADOVA01).

Data Availability Statement: The original contributions presented in the study are included in the article, further inquiries can be directed to the corresponding author.

Acknowledgments: We would like to express our recognition of the fundamental work at the HIBRI2 project of the Cuban Center for Information Management and Energy Development (CUBAENERGÍA) as well as the NGO Cuban Society for the Promotion of Renewable Energy Sources and Respect for the Environment (CUBASOLAR). Special thanks to the people of Guasasa and the municipality's authorities.

Conflicts of Interest: The authors declare no conflicts of interest.

References

1. IEA, SDG7: Data and Projections. https://www.iea.org/reports/sdg7-data-and-projections (accessed on 10 August 2024).
2. Domínguez Bravo, J., Los sistemas de información geográfica en la planificación e integración de energías renovables. CIEMAT: Madrid, 2002; p 159.
3. Domínguez, J.; Arribas, L.; Diego, L. d.; Herrera, I.; Zarzalejo, L. Sistema integrado de control para el abastecimiento de energía mediante sistemas híbridos en comunidades aisladas de Cuba. Fase II (proyecto HIBRI2) 1520; CIEMAT: Madrid, 2022; p 62. . https://www.ciemat.es/portal.do?TR=A&IDR=1&identificador=1046
4. Domínguez, J.; Bellini, C.; Arribas, L.; Amador, J.; Torres-Pérez, M.; Martín, A. M., IntiGIS-Local: A Geospatial Approach to Assessing Rural Electrification Alternatives for Sustainable Socio-Economic Development in Isolated Communities—A Case Study of Guasasa, Cuba. *Energies* **2024,** 17, (15), 3835. https://doi.org/10.3390/en17153835
5. Benalcazar, P.; Komorowska, A.; Kamiński, J., A GIS-based method for assessing the economics of utility-scale photovoltaic systems. *Appl Energ* **2024,** 353, 122044. https://doi.org/10.1016/j.apenergy.2023.122044
6. Gacu, J. G.; Garcia, J. D.; Fetalvero, E. G.; Catajay-Mani, M. P.; Monjardin, C. E. F., Suitability Analysis Using GIS-Based Analytic Hierarchy Process (AHP) for Solar Power Exploration. In *Energies*, 2023; Vol. 16. https://doi.org/10.3390/en16186724
7. Ibraheem, I. F., Remote sensing data and environmental parameters usage for the establishment of a mapping of solar energy potential in Iraq. *AIP Conference Proceedings* **2023,** 2787, (1). https://doi.org/10.1063/5.0149069
8. Kanters, J.; Wall, M.; Kjellsson, E., The Solar Map as a Knowledge Base for Solar Energy Use. *Energy Procedia* **2014,** 48, (0), 1597-1606. https://doi.org/10.1016/j.egypro.2014.02.180
9. Loquias, R.; Palima, N.; Juanillas, M.; Magno, L.; Compuesto, K.; Zagada, A.; Isaac, V.; Tabal, K. M.; Terano, H. J., Suitability Mapping of Solar Energy Potential of Selected Areas in Camarines Sur using ArcGIS. *Journal of Engineering and Emerging Technologies* **2022,** 1, 37-49. https://doi.org/10.52631/jeet.v1i1.185
10. Szabó, Z.; Wang, G.; Ágnes, S., Estimating Solar Energy Potential of Hungary Based on Raster Maps. *Journal of Digital Landscape Architecture* **2023**, (8), 112-123. https://doi.org/10.14627/537740013
11. S. Alrwashdeh, S.; M. Alsaraireh, F.; A. Saraireh, M., Solar radiation map of Jordan governorates. *International Journal of Engineering & Technology* **2018,** 7, (3), 1664. https://doi.org/10.14419/ijet.v7i3.15557
12. Settou, B.; Settou, N.; Gouareh, A.; Negrou, B.; Mokhtara, C.; Messaoudi, D., A high-resolution geographic information system-analytical hierarchy process-based method for solar PV power plant site selection: a case study Algeria. *Clean Technologies and Environmental Policy* **2020,** 23, (1), 219-234. https://doi.org/10.1007/s10098-020-01971-3
13. Hasan, A. S. M. M.; Kesapabutr, P.; Möller, B., Bangladesh's pathways to net-zero transition: Reassessing country's solar PV potential with high-resolution GIS data. *Energy for Sustainable Development* **2024,** 81, 101511. https://doi.org/10.1016/j.esd.2024.101511
14. Yaiche, M. R.; Bouhanik, A.; Bekkouche, S. M. A.; Malek, A.; Benouaz, T., Revised solar maps of Algeria based on sunshine duration. *Energy Convers Manage* **2014,** 82, 114-123. https://doi.org/10.1016/j.enconman.2014.02.063
15. Enjavi-Arsanjani, M.; Hirbodi, K.; Yaghoubi, M., Solar Energy Potential and Performance Assessment of CSP Plants in Different Areas of Iran. *Energy Procedia* **2015,** 69, 2039-2048. https://doi.org/10.1016/j.egypro.2015.03.216
16. Jung, J.; Han, S.; Kim, B., Digital numerical map-oriented estimation of solar energy potential for site selection of photovoltaic solar panels on national highway slopes. *Appl Energ* **2019,** 242, 57-68. https://doi.org/10.1016/j.apenergy.2019.03.101

17. Kanters, J.; Wall, M., A planning process map for solar buildings in urban environments. *Renew Sustain Energy Rev* **2016,** 57, 173-185. https://doi.org/10.1016/j.rser.2015.12.073
18. Wegertseder, P.; Lund, P.; Mikkola, J.; García Alvarado, R., Combining solar resource mapping and energy system integration methods for realistic valuation of urban solar energy potential. *Sol Energy* **2016,** 135, 325-336. https://doi.org/10.1016/j.solener.2016.05.061
19. ESRI, ArcGIS for Desktop 10.8. https://www.esri.com/en-us/arcgis/products/arcgis-desktop/overview (accessed on 10 August 2024).
20. Meteotest, Meteonorm Software. Worldwide irradiation data. https://meteonorm.com/en/ (accessed on 10 August 2024).
21. EcuRed, Guasasa. https://www.ecured.cu/Guasasa (accessed on 10 August 2024).
22. Prăvălie, R.; Patriche, C.; Bandoc, G., Spatial assessment of solar energy potential at global scale. A geographical approach. *Journal of Cleaner Production* **2019,** 209, 692-721. https://doi.org/10.1016/j.jclepro.2018.10.239
23. Ali, S.; Taweekun, J.; Techato, K.; Waewsak, J.; Gyawali, S., GIS based site suitability assessment for wind and solar farms in Songkhla, Thailand. *Renew Energy* **2019,** 132, 1360-1372. https://doi.org/10.1016/j.renene.2018.09.035
24. Mahtta, R.; Joshi, P. K.; Jindal, A. K., Solar power potential mapping in India using remote sensing inputs and environmental parameters. *Renew Energy* **2014,** 71, (0), 255-262. https://doi.org/10.1016/j.renene.2014.05.037
25. Pavlovic, T. M.; Milosavljevic, D. D.; Mirjanic, D.; Pantic, L. S.; Radonjic, I. S.; Pirsl, D., Assessments and perspectives of PV solar power engineering in the Republic of Srpska (Bosnia and Herzegovina). *Renew Sustain Energy Rev* **2013,** 18, 119-133. https://doi.org/10.1016/j.rser.2012.10.007b
26. Solargis, Global Solar Atlas. https://globalsolaratlas.info (accessed on 10 August 2024).
27. NASA, Prediction of Wordwide Energy Resources. https://power.larc.nasa.gov/ (accessed on 10 August 2024).
28. European Commission, Photovoltaic Geographical Information System (PVGIS). https://joint-research-centre.ec.europa.eu/photovoltaic-geographical-information-system-pvgis_en (accessed on 10 August 2024).
29. Lukač, N.; Žlaus, D.; Seme, S.; Žalik, B.; Štumberger, G., Rating of roofs' surfaces regarding their solar potential and suitability for PV systems, based on LiDAR data. *Appl Energ* **2013,** 102, (0), 803-812. https://doi.org/10.1016/j.apenergy.2012.08.042
30. Antonanzas, J.; Urraca, R.; Martinez-de-Pison, F. J.; Antonanzas-Torres, F., Solar irradiation mapping with exogenous data from support vector regression machines estimations. *Energy Convers Manage* **2015,** 100, 380-390. https://doi.org/10.1016/j.enconman.2015.05.028
31. Srećković, N.; Lukač, N.; Žalik, B.; Štumberger, G., Determining roof surfaces suitable for the installation of PV (photovoltaic) systems, based on LiDAR (Light Detection And Ranging) data, pyranometer measurements, and distribution network configuration. *Energy* **2016,** 96, 404-414. http://dx.doi.org/10.1016/j.energy.2015.12.078
32. Martín, A. M.; Dominguez, J., Solar Radiation Interpolation. In *Solar Resources Mapping: Fundamentals and Applications*, Polo, J.; Martín-Pomares, L.; Sanfilippo, A., Eds. Springer International Publishing: Cham, Switzerland, 2019; pp 221-242. https://doi.org/10.1007/978-3-319-97484-2_8
33. ESRI, ArcGIS Desktop. ArcMap. Area Solar Radiation. https://desktop.arcgis.com/en/arcmap/latest/tools/spatial-analyst-toolbox/area-solar-radiation.htm (accessed on 10 August 2024).
34. Santos, T.; Gomes, N.; Freire, S.; Brito, M. C.; Santos, L.; Tenedório, J. A., Applications of solar mapping in the urban environment. *Applied Geography* **2014,** 51, 48-57. https://doi.org/10.1016/j.apgeog.2014.03.008
35. Kausika, B. B.; van Sark, W. G. J. H. M., Calibration and Validation of ArcGIS Solar Radiation Tool for Photovoltaic Potential Determination in the Netherlands. *Energies* **2021,** 14, (7), 1865. https://doi.org/10.3390/en14071865
36. Hofierka, J.; Šúri, M.; Huld, T. r.sun. Solar irradiance and irradiation model. https://grass.osgeo.org/grass80/manuals/r.sun.html (accessed on 10 August 2024).
37. Li, Z. Q.; Zhang, Z. D.; Davey, K., Estimating Geographical PV Potential Using LiDAR Data for Buildings in Downtown San Francisco. *Transactions in Gis* **2015,** 19, (6), 930-963. https://doi.org/10.1111/tgis.12140
38. Teves, J.; Sola, E. F.; Pintor, B. H.; Ang, M. R. C. In Assessing the urban solar energy resource potential of Davao City, Philippines, using LiDAR Digital Surface Model (DSM) and GRASS GIS, 2016; 2016; pp 1000809-1000809-12. http://dx.doi.org/10.1117/12.2241407
39. Fu, P.; Rich, P. M. In *Design and implementation of the Solar Analyst: an ArcView extension for modeling solar radiation at landscape scales*, Proceedings of the 19th Annual ESRI User Conference, San Diego, USA, 1999; San Diego, USA, 1999. . http://gis.esri.com/library/userconf/proc99/proceed/papers/pap867/p867.htm
40. Duffie, J. A.; Beckman, W. A.; Blair, N., *Solar engineering of thermal processes. Photovoltaics and wind*. 5th ed.; John Wiley & Sons: Hoboken, NJ, USA, 2020.

 doi:10.20944/preprints202408.1615.v1

41. Iqbal, M., *An introduction to solar radiation*. Academic Press Canada: 1983.
42. Wald, L., Basics in solar radiation at Earth surface - Revised version. In MINES ParisTech: 2019. https://minesparis-psl.hal.science/hal-02164311
43. Muneer, T., *Solar radiation and daylight models*. Elsevier Butterworth-Heinemann: Oxford, UK, 2004.
44. World Radiation Centre. https://www.pmodwrc.ch/en/home/ (accessed on 10 August 2024).
45. Goswami, Y.; Kreith, F.; Kreider, J. F., *Principles of solar engineering*. Taylor & Francis: Philadelphia, USA, 1999.
46. Kasten, F.; Young, A. T., Revised optical air mass tables and approximation formula. *Appl. Opt.* **1989,** 28, (22), 4735-4738. http://dx.doi.org/10.1364/AO.28.004735
47. Cebecauer, T.; Huld, T. A.; Šúri, M. In *High resolution digital elevation model for improved PV yield estimates*, Proceedings of the 22nd European Photovoltaic Solar Energy Conference, Milán (Italia), 2007; Milán (Italia), 2007; pp 3553-3557. https://publications.jrc.ec.europa.eu/repository/handle/JRC36425
48. JAXA, ALOS Global Digital Surface Model. https://www.eorc.jaxa.jp/ALOS/en/dataset/aw3d30/aw3d30_e.htm (accessed on 10 August 2024).
49. Alves, M.; Sanches, L.; Nogueira, J.; Silva, V., Effects of Sky Conditions Measured by the Clearness Index on the Estimation of Solar Radiation Using a Digital Elevation Model. *Atmospheric and Climate Sciences* **2013,** 3, (4), 618-626. https://doi.org/10.4236/acs.2013.34064
50. Liu, B. Y. H.; Jordan, R. C., The interrelationship and characteristic distribution of direct, diffuse and total solar radiation. *Sol Energy* **1960,** 4, (3), 1-19. https://doi.org/10.1016/0038-092X(60)90062-1
51. Mora-López, L.; Piliougine, M.; Carretero, J. E.; Sidrach-de-Cardona, M., Integration of Statistical and Machine Learning Models for Short-term Forecasting of the Atmospheric Clearness Index. In *5th International Congress on Environmental Modelling and Sorftware*, Ottawa, Ontario, Canada, 2010. https://scholarsarchive.byu.edu/iemssconference/2010/all/506/
52. Singh, J.; Bhattacharya, B. K.; Kumar, M.; Mallick, K., Modelling monthly diffuse solar radiation fraction and its validity over the Indian sub-tropics. *Int. J. Climatol.* **2013,** 33, (1), 77-86. https://doi.org/10.1002/joc.3408
53. Meteonorm, METEONORM Global Meteorological Database. Handbook Part II. Theory. 2012.
54. Perez, R.; Ineichen, P.; Seals, R.; Michalsky, J.; Stewart, R., Modeling daylight availability and irradiance components from direct and global irradiance. *Sol Energy* **1990,** 44, (5), 271-289. https://doi.org/10.1016/0038-092X(90)90055-H
55. Meehl, G.; Stocker, T.; Collins, W. D.; Friedlingstein, P.; Gaye, A. T.; Gregory, J. M.; Kitoh, A.; Knutti, R.; Murphy, J. M.; Noda, A.; Raper, S. C. B.; Watterson, I. G.; Weaver, A. J.; Zhao, Z.-C., Global climate projections climate change 2007: The physical science basis. *The Physical Science Basis* **2007**, 747-845.
56. ESRI, ArcGIS Desktop. ArcMap. Points Solar Radiation. https://desktop.arcgis.com/en/arcmap/latest/tools/spatial-analyst-toolbox/points-solar-radiation.htm (accessed on 10 August 2024).